PCCP

NMR studies of phosphorus chalcogenide–copper iodide coordination compounds

Gunther Brunklaus,[a] Jerry C. C. Chan,[a] Hellmut Eckert,*[a] Sara Reiser,[b] Tom Nilges[b] and Arno Pfitzner*[b]

[a] *Institut für Physikalische Chemie, Westfälische Wilhelms-Universität Münster, Schlossplatz 7, D-48149 Münster, Germany*
[b] *Institut für Anorganische Chemie, Universität Regensburg, D-93040 Regensburg, Germany*

Received 31st March 2003, Accepted 1st July 2003
First published as an Advance Article on the web 30th July 2003

The local structures of the new phosphorus chalcogenide – copper iodide coordination compounds $(CuI)P_4Se_4$, $(CuI)_2P_8Se_3$, $(CuI)_3P_4Se_4$, and $(CuI)_3P_4S_4$ are investigated using comprehensive ^{63}Cu, ^{65}Cu, and ^{31}P magic angle spinning NMR techniques. Peak assignments are proposed on the basis of homo- and heteronuclear indirect spin–spin interactions, available from lineshape analysis and/or two-dimensional correlation spectroscopy. In particular, the ^{31}P-$^{63,65}Cu$ scalar coupling constants have been extracted from detailed lineshape simulations of the ^{31}P resonances associated with the Cu-bonded P atoms. In addition, the RN_n^ν pulse symmetry concept of Levitt and coworkers has been utilized for total through-bond correlation spectroscopy (TOBSY) of directly-bonded phosphorus species. The resonance assignments obtained facilitate a discussion of the ^{31}P and $^{63,65}Cu$ NMR Hamiltonian parameters in terms of the detailed local atomic environments. Analysis of the limited data set available for this group of closely related compounds offers the following conclusions: (1) bonding of a special phosphorus site in a given P_4X_n (X = S, Se) molecule to Cu^+ ions shifts the corresponding ^{31}P NMR signal upfield by about 50 ppm relative to the uncomplexed molecule, (2) the magnitude of the corresponding scalar ^{31}P-$^{63,65}Cu$ spin–spin coupling constant tends to decrease with increasing Cu–P distance, and (3) the $^{63,65}Cu$ nuclear electric quadrupolar coupling constants appear to be weakly correlated with the shear strain parameter specifying the degree of local distortion present in the four-coordinated $[CuI_2P_2]$ and $[CuI_3P]$ environments. Overall, the results illustrate the power and potential of advanced solid state NMR methodology to provide useful structural information in this class of materials.

Introduction

The use of copper(I) halides as a preparative tool has recently been reported to be a successful strategy to compounds showing enhanced ionic conductivity.[1,2] Along this route a new class of solid state materials has been generated in which phosphorus chalcogenide cages are being stabilized as copper iodide coordination compounds. This list includes the well known cage structures $P_4S(e)_3$,[3–9] *catena*-P_4Se_4,[10] and β-P_4S_4,[9,11] but also the hitherto unknown molecules P_8Se_3,[12] and β-P_4Se_4.[13] While all of the above materials have been structurally characterized by single-crystal X-ray diffraction, this method requires suitable crystals and cannot be applied to microcrystalline or even amorphous materials. Therefore, it is also of great interest to develop and utilize the potential of alternative experimental approaches with structural information content. In this regard, solid state nuclear magnetic resonance (NMR) spectroscopy provides an element-selective, inherently quantitative method that can offer very detailed insights into the local environments, bond connectivities, as well as structural or dynamic disorder of the building units involved.[11,13] In the present contribution we will discuss the utility of one- and two-dimensional ^{31}P and $^{63,65}Cu$ NMR to characterize these features and reveal details on the interaction between the phosphorus chalcogenide cages and their more or less ionic environments. The crystallographically distinct phosphorus sites in these compounds are in general well-resolvable on the basis of their isotropic chemical shifts, obtained from the magic-angle spinning spectra. Since, unfortunately, the theoretical understanding of the chemical shifts measured in phosphorus chalcogenides is only poorly developed, the recovery and analysis of dipole-dipole and scalar interactions is of particular significance for peak assignments. Important information stems from the characteristic peak multiplet structures arising from heteronuclear indirect spin–spin interactions of the ^{31}P nuclei with the $^{63,65}Cu$ isotopes, which were first analyzed in detail in various Cu-phosphine complexes.[14,15] Complementary insights into direct dipole–dipole interactions are accessible from $^{31}P\{^{63}Cu\}$ rotational echo adiabatic passage double resonance (REAPDOR) NMR studies.[16] For probing homonuclear ^{31}P–^{31}P couplings a wide variety of dipolar recoupling techniques have been developed.[17,18] For improved spectral selectivity, however, it is useful to focus on the analysis of indirect (scalar) spin–spin interactions, which can discriminate through-bond connectivity from mere spatial proximity. Thus, a variety of two-dimensional total-through-bond correlation spectroscopic (TOBSY) approaches have been described in the literature,[19–27] enabling the selective correlation between those nuclei that are directly bonded. A particularly successful general concept for the development of suitable recoupling strategies has been the so-called RN_n^ν pulse symmetry, introduced by Levitt and co-workers.[28,29] Thanks to the flexibility and powerful features offered by this class of pulse sequences, some of the RN_n^ν pulse symmetries are well suited for TOBSY-like experiments. As previously shown in our laboratory, an extremely promising pulse symmetry for TOBSY-like experiments, which is rather insensitive to resonance offsets and experimental imperfections, is determined to be $R30_6^{14}$.[30]

 DOI: 10.1039/b303610n

This journal is © The Owner Societies 2003

Simulations using the SIMPSON software package[31] and validation experiments conducted on crystalline model compounds[32] have shown that R-TOBSY is fairly insensitive to the presence of through-space dipolar couplings, to the details of mutual spin tensor orientations, to large resonance offsets, and to experimental imperfections such as pulse power misadjustments and/or radio frequency inhomogeneities.[30,32] These favourable properties are particularly advantageous for connectivity studies in phosphorus chalcogenide systems, which are quite generally characterized by wide spectral dispersions. It is the purpose of this study to explore the applicability of R-TOBSY as an assignment tool in the present class of coordination compounds, to extract their relevant NMR Hamiltonian parameters and to discuss their structural interpretation in conjunction with known crystallographic information. A preliminary account of results on $(CuI)_3P_4S_4$ has been given previously[11] and will be expanded upon in the present work.

Experimental

The following compounds were included in this study: $(CuI)P_4Se_4$, $(CuI)_2P_8Se_3$, $(CuI)_3P_4Se_4$, and $(CuI)_3P_4S_4$. These materials were prepared by standard high-temperature high-vacuum techniques, following the previously published procedures.[10–13] Compound purity was ascertained using standard X-ray powder diffraction and magic-angle spinning NMR methods. Solid state ^{63,65}Cu and ^{31}P NMR spectra were obtained on Bruker DSX 400 and DSX 500 NMR spectrometers equipped with suitable magic-angle spinning (MAS) NMR probes. Samples were rotated in 2.5 or 4 mm zirconia rotors at spinning frequencies up to 30 kHz. Additional low-field NMR spectra were recorded in a 4.7 T magnet. Typical $\pi/2$-pulse lengths were set to 2–3 μs, except for ^{63,65}Cu spectra, which were measured with selective $\pi/2$-pulses of 1 μs duration. If not stated otherwise, all spectra were recorded as rotor-synchronized spin echoes avoiding severe baseline distortions. Data analyses and lineshape simulations were carried out using the DMFIT[33] and WSOLIDS1[34] simulation packages. Chemical shift references were solid CuI and 85% H_3PO_4, respectively. Fig. 1 shows the R-TOBSY pulse sequence as used in the present study to probe direct ^{31}P-^{31}P bond connectivities. Following an excitation of single quantum coherence by a simple $\pi/2$-pulse, the system evolves under the MAS Hamiltonian during the evolution period t_1, which is then terminated by the second $\pi/2$-pulse. The mixing period comprises k cycles of RN_n^ν pulse symmetry causing coherence transfer between spins coupled by sufficiently strong indirect spin–spin interactions. Further details of the pulse sequence are described elsewhere.[30] Two-dimensional R-TOBSY NMR experiments were carried out with the above spectrometer hardware at 4.7 T, 9.4 T, and 11.7 T, using an rf nutation frequency of five times the MAS rotation frequency. In one case, an additional three-step supercycle for enhanced zero-quantum filtering was included applying $2\pi/3$ phase shifts to each basic $R30_6^{14}$ block.[35] Detailed experimental conditions are given in the corresponding figure captions. Mixing times were optimized on the basis of one- or two-dimensional coherence transfer experiments. Quadrature detection in the F1-dimension was achieved by the hypercomplex approach (STATES method).[36] Saturation combs were applied before the relaxation delays for all experiments.

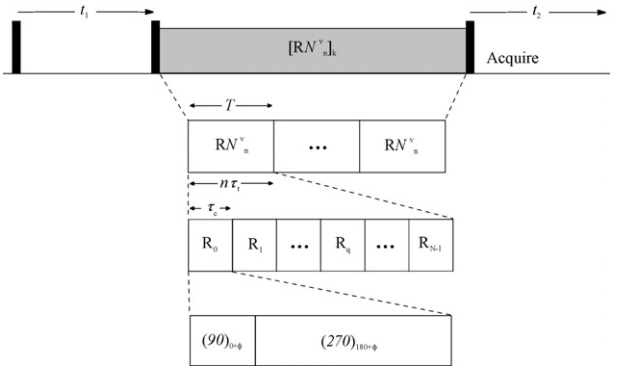

Fig. 1 The RN_n^ν pulse sequence in the context of TOBSY experiments. The three rectangular blocks in black represent $\pi/2$ pulses. The mixing period sandwiched by the second and third $\pi/2$ pulses comprise k cycles of RN_n^ν pulse symmetry.

Results

1. $(CuI)P_4Se_4$

The structure of this compound is characterized by neutral polymeric P_4Se_4 strands which are linked by copper atoms thereby forming layers parallel to (010) (*cf.* Fig. 2a). The strands themselves consist of norbornane-type P_4Se_3 cages comprised of P_2-dumbbells connected by selenium atoms. In addition, the cages are bridged by exocyclic selenium atoms revealing P_4Se_4 polymers, which are attached to copper atoms exclusively by the bridgehead phosphorus atoms as is illustrated in Fig. 2b. The distorted tetrahedral environment of the copper atoms is completed by iodine atoms. Fig. 3 shows the ^{63}Cu solid state MAS NMR spectrum, reflecting strong second-order quadrupolar perturbations arising from the local electric field gradients (EFG) present at the copper site. Table 1 summarizes the ^{63}Cu NMR lineshape parameters obtained by the DMFIT routine for all of the compounds investigated here. ^{65}Cu NMR data recorded for comparison were found to be consistent with the intrinsic difference of the quadrupolar moments of both Cu isotopes ($eQ(^{63}Cu) = 1.6 \times 10^{-33}$ m^2, $eQ(^{65}Cu) = 1.5 \times 10^{-33}$ m^2, $\Delta eQ \approx 6.7\%$). The ^{77}Se MAS spectrum (data not shown) of $(CuI)P_4Se_4$ reveals three peaks at $\delta = -588$ ppm, $\delta = -790$ ppm and $\delta = -858$ ppm. Within the experimental errors, the integrated area ratio was found to be 1:2:1, which clearly confirms the three crystallographically

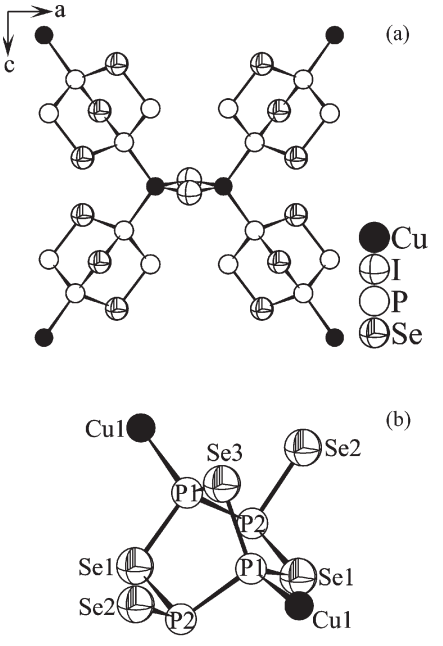

Fig. 2 (a) Crystal structure of $(CuI)P_4Se_4$ shown as a projection along the b axis. P_4Se_4 strands are linked by copper atoms producing layers parallel to (010). (b) The basic building block: a norbornane-type P_4Se_3 cage bridged by selenium atoms. Exclusively the bridgehead phosphorus atoms are bonded to copper.

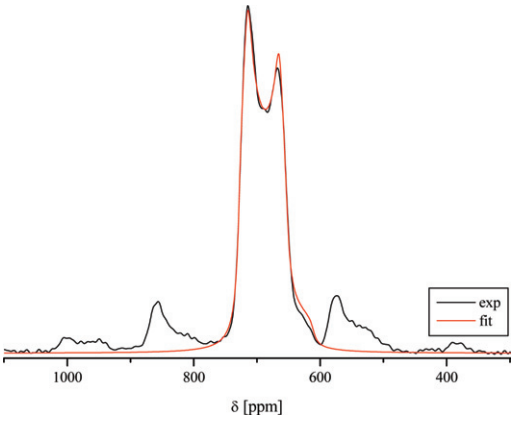

Fig. 3 ^{63}Cu MAS spectrum of $(CuI)P_4Se_4$ at 9.4 T (106.08 MHz) and a spinning frequency of 15 kHz. The minor peaks are spinning side bands.

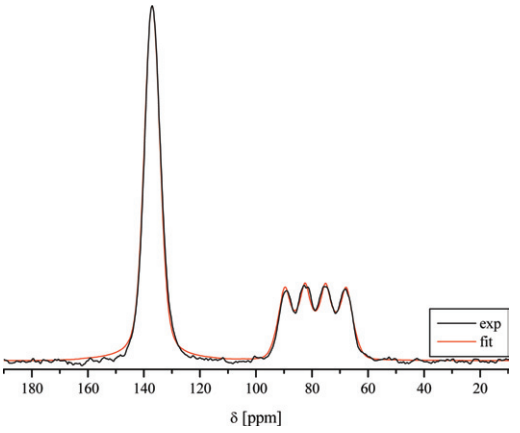

Fig. 4 ^{31}P MAS spectrum of $(CuI)P_4Se_4$ at 7.1 T (121.49 MHz) and a spinning frequency of 30 kHz.

distinct selenium sites. Hence, the resonance at $\delta = -790$ ppm can be assigned to the selenium site Se1 whereas further peak assignments remain impossible at this stage.

The ^{31}P MAS-NMR spectrum (*cf.* Fig. 4) consists of two main resonances centered at $\delta_{(P1)} = 78.7$ ppm and $\delta_{(P2)} = 137.0$ ppm, respectively, with an integrated area ratio of $\approx$1:1. The peak assigned to the crystallographic phosphorus site P1 is split into a multiplet due to the residual dipolar and scalar couplings to the quadrupolar ^{63}Cu and ^{65}Cu nuclei associated with the directly bonded Cu1 site. Using WSOLIDS1, the lineshape for the multiplet is simulated as a sum of two components reflecting the ^{63}Cu/^{65}Cu isotopic abundance ratio of 69.1%/30.9% $\approx$ 2.236. Furthermore, in agreement with typical literature data,[15] the anisotropy ΔJ of the indirect dipole–dipole interaction tensor was held fixed at 500 Hz for all of the compounds studied. With the particular set of interaction parameters relevant here, variations of ΔJ by 100% had no significant effect on the simulated lineshapes. The values for the dipolar coupling constants given in Table 2 are readily computed from the crystal structure, whereas the isotropic J values were obtained *via* lineshape fitting, using the quadrupolar coupling parameters determined independently from the Cu NMR spectra and the additional constraint that $^1J(^{63}Cu–^{31}P)/^1J(^{65}Cu–^{31}P) = \gamma(^{63}Cu)/\gamma(^{65}Cu)$. Since there is no independent knowledge concerning the mutual orientations of the Cu-electric field gradient axes with respect to the Cu–P interaction tensor, the corresponding Euler angles α, β and γ were systematically varied. The multiplet intensity

Table 1 ^{63}Cu and/or ^{65}Cu NMR isotropic chemical shifts δ_{iso} ($\pm$2 ppm), nuclear electric quadrupolar coupling constant C_Q ($\pm$0.2 MHz) and electric field gradient asymmetry parameter η ($\pm$0.1) obtained on the phosphorus chalcogenide-copper iodide coordination compounds. All the data are from MAS, and for $(CuI)_2P_8Se_3$ additional data obtained from the static spectra are included in parentheses. Also listed is the shear strain parameter χ (defined in the text) computed from the crystal structure

Site	δ_{iso}/ppm	C_Q [MHz]	η	χ
$(CuI)P_4Se_4$				
^{63}Cu1	740	4.8	0.18	0.52
^{65}Cu1	735	4.6	0.14	0.52

Site	δ_{iso}/ppm	C_Q/MHz	η	χ	%
$(CuI)_2P_8Se_3$					
Cu1	815 (790)	10.7 (9.3)	0.15 (0.10)	0.63	58 (45)
Cu2	626 (751)	6.3 (7.2)	0.27 (0.27)	0.41	42 (55)

Site	δ_{iso}/ppm	C_Q/MHz	η	χ	%
$(CuI)_3P_4Se_4$					
Cu1	408	4.3	0.39	0.30	28
Cu2	300	5.9	0.20	0.47	37
Cu3	305	6.6	0.13	0.50	35

Site	δ_{iso}/ppm	C_Q/MHz	η	χ	%
$(CuI)_3P_4S_4$					
^{63}Cu1	419	2.84	0.50	0.29	31
^{63}Cu2	331	7.04	0.03	0.43	69
^{65}Cu1	415	2.75	0.55	0.29	33
^{65}Cu2	337	6.89	0.17	0.43	67

Table 2 ^{31}P NMR Hamiltonian parameters δ_{iso} ($\pm$1 ppm) and $^1J_{iso}(^{31}P\text{-}^{63,65}Cu)$($\pm$10 Hz)obtained on the phosphorus chalcogenide–copper iodide coordination compounds. Dipolar coupling constants D are calculated from known internuclear distances.

Sites/spin pairs	δ_{iso}/ppm	D/Hz	J_{iso}/Hz	%
$(CuI)P_4Se_4$				
P1–^{63}Cu	78.7	1090	867	34.6
P1–^{65}Cu	78.7	1167	928	15.4
P2	137.0	—	—	50

Sites	δ_{iso}/ppm	%
$(CuI)_2P_8Se_3$		
P1(P1′)	−44	23
P2(P2′)	94	24
P3(P3′)	83.6	27
P4(P4′)	105.2	26

Sites/spin pairs	δ_{iso}/ppm	D/Hz	J_{iso}/Hz	%
$(CuI)_3P_4Se_4$				
P1–^{63}Cu1	120.2	1143	1210	17.5
P1–^{65}Cu1	120.2	1224	1297	7.5
P4–^{63}Cu2	135.9	1132	1200	19.2
P4–^{65}Cu2	136.1	1212	1286	8.3
P2–^{63}Cu3	133.0	1112	1100	15.7
P2–^{65}Cu3	133.0	1190	1178	6.8
P3	78.4	—	—	25

Sites/spin pairs	δ_{iso}/ppm	D/Hz	J_{iso}/Hz	%
$(CuI)_3P_4S_4$				
P1–^{63}Cu1	144.9	1176	1200	17.1
P1–^{65}Cu1	144.9	1258	1284	7.7
P2–^{63}Cu2	117.3	1154	1200	34.2
P2–^{65}Cu2	117.3	1235	1284	15.3
P3	83.0	—	—	25.7

distributions were found to be only marginally affected by these parameters and consequently, we assumed $\alpha = \beta = \gamma = 45°$ in all simulations to represent the most general case. The final simulation results for all four compounds are summarized in Table 2. Fig. 5 demonstrates the P1–P2 connectivity in $(CuI)P_4Se_4$ using the two-dimensional R-TOBSY experiment. Successful coherence transfer *via* the scalar coupling is illustrated by the crosspeaks linking the two resonances. The spectrum confirms that the presence of the dominant ^{31}P–$^{63,65}Cu$ heteronuclear scalar interactions does not interfere with the applicability of R-TOBSY of achieving homonuclear coherence transfer between the directly bonded ^{31}P spins.

2. $(CuI)_2P_8Se_3$

The crystal structure of this compound consists of planar Cu_2I_2 rhomboids and novel P_8Se_3 cages arranged in layers parallel to (001) as depicted in Fig. 6.[12] The P_8Se_3 cage can in principle be derived from a P_8 cube by inserting selenium atoms into the three edges related by a threefold axis of the cube. Due to the crystallographic packing effects, however, the intrinsic D_3 symmetry of the P_8Se_3 cage molecule is reduced to C_2 symmetry. Since both the copper and iodine atoms are crystallographically inequivalent, a slight deviation from an ideal rhomboid is present while the coordination of four phosphorus atoms of the P_8Se_3 cage to two copper atoms with a P–Cu distance of about 228 pm is a similar motif as previously found for $(CuI)P_4Se_4$.

The static ^{63}Cu spinecho-NMR spectrum shown in Fig. 7 reflects strong second-order quadrupolar perturbations owing to the local electric field gradients (EFGs) present at both copper sites. Their isotropic chemical shifts are quite similar producing strong overlap even at high magnetic field strengths. Nevertheless, the lineshape analysis of the ^{63}Cu spectrum of $(CuI)_2P_8Se_3$ clearly uncovers the inequivalence of both copper sites with an integrated area ratio of about 1:1 revealing strongly different quadrupolar coupling constants: Resonance A is characterized by $\delta_{CS} = 790$ ppm, $C_Q = 9.3$ MHz and $\eta = 0.10$, whereas signal B is characterized by $\delta_{CS} = 751$ ppm, $C_Q = 7.2$ MHz and $\eta = 0.27$. Tentatively, we assign resonance A to the more distorted Cu site Cu1, and resonance B to Cu2. Fig. 7b shows the corresponding MAS-NMR spectrum along with the peak deconvolution. While the quadrupolar coupling constants obtained are roughly consistent with those measured from the static spectrum, we note a significant

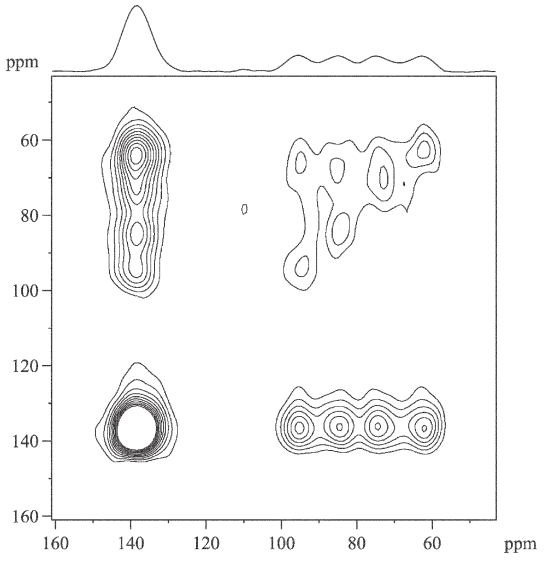

Fig. 5 ^{31}P-12 kHz MAS SC-R-TOBSY spectrum of $(CuI)P_4Se_4$ at 4.7 T (81.02 MHz) under the following experimental conditions: $\tau_{mix} = 12.0$ ms, 40 t_1 increments at steps of 83.33 μs, relaxation delay 30 s. Quadrature detection in the F_1 dimension was achieved by the hypercomplex approach (STATES). Ten positive contour levels between 5% and 40% of the maximum peak intensity are plotted. The F_2 projection is shown on the top.

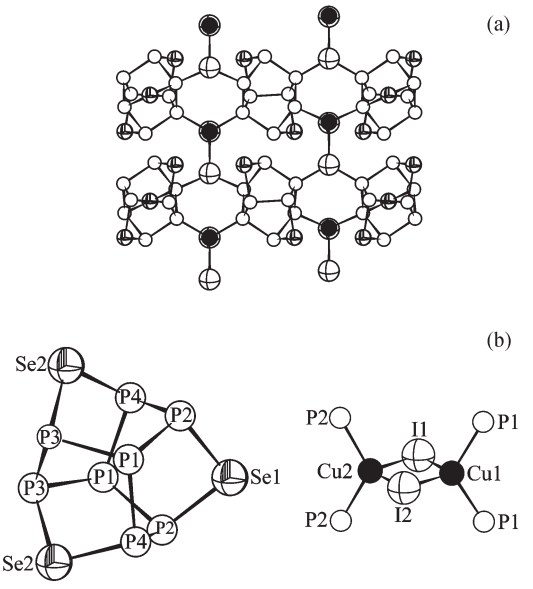

Fig. 6 (a) A projection along the *a*-axis of the crystal structure of $(CuI)_2P_8Se_3$. The P_8Se_3 cages and the Cu_2I_2 rhomboids are arranged in layers parallel to (001). Only half of the phosphorus atoms are attached to copper. (b) The basic units: the novel P_8Se_3 cage and the Cu_2I_2 rhomboid.

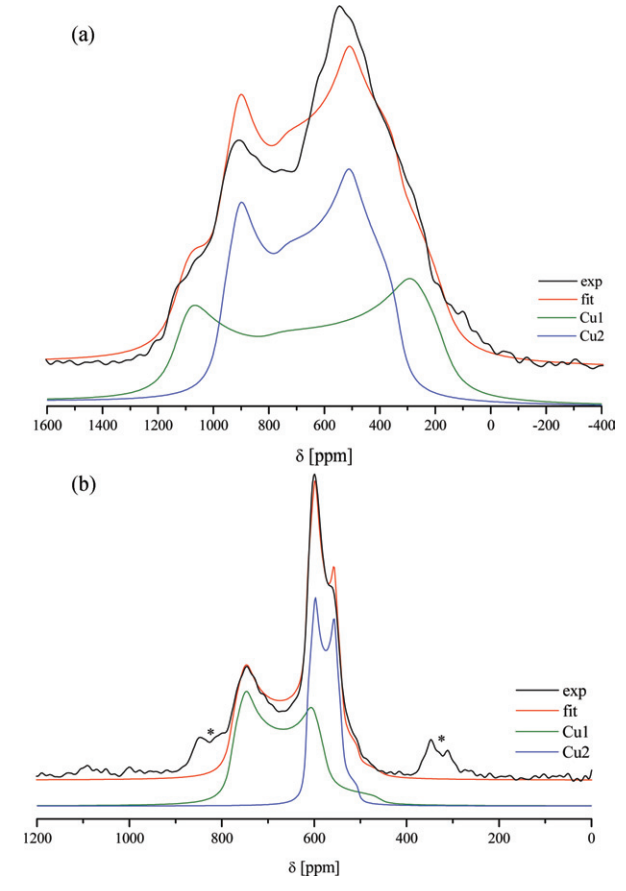

Fig. 7 ^{65}(a) Cu static spinecho spectrum of $(CuI)_2P_8Se_3$ at 9.4 T (113.70 MHz). The evolution time was set to 20 μs. Below the individual lineshapes of the two copper sites present are given. (b) 35 kHz ^{65}Cu-MAS NMR spectrum of $(CuI)_2P_8Se_3$ at 11.7 T (142.01 MHz). The contributions of both copper sites are given. Spinning sidebands are marked with asteriks.

discrepancy for the isotropic chemical shift value of the Cu2 site between both measurements. This experimental uncertainty, documented in Table 1, might arise from the fact that the static spectrum is also affected by chemical shift anisotropy effects distorting the second-order quadrupolar lineshape.

The four distinct phosphorus atoms give rise to separate peaks in the ^{31}P MAS-NMR spectrum of $(CuI)_2P_8Se_3$, which are, however, not completely resolved from each other (data not shown). Furthermore, unlike the situation in $(CuI)P_4Se_4$, the peak splittings arising from ^{31}P-^{63,65}Cu scalar coupling are not clearly evident. This result may either reflect weaker ^{31}P-^{63,65}Cu scalar interactions than in $(CuI)P_4Se_4$ or more rapid spin fluctuations limiting the lifetimes of the ^{63,65}Cu Zeeman states. Still, it appears likely that the significant broadening of the ^{31}P resonance at $\delta = -44.0$ ppm arises from unresolved scalar couplings, suggesting an assignment to one of the copper coordinated phosphorus sites P1(P1′) or P2(P2′). This suggestion can be independently checked by probing the ^{63}Cu –^{31}P heteronuclear dipole-dipole interactions. Successful dipolar recoupling to quadrupolar nuclei is accomplished by the REAPDOR sequence[16] predicting a noticeable drop of signal intensity of those ^{31}P resonances associated with the sites P1(P1′) and P2(P2′), when the copper spins are irradiated during the rotor cycle. Generally, both copper isotopes are suitable, but owing to the larger natural abundance of the ^{63}Cu isotope, the ^{31}P{^{63}Cu}-REAPDOR experiment is preferred. Fig. 8 presents a typical result. The extent of signal attenuation depends on both the magnitude of the quadrupolar coupling constant and on the ability of the recoupling pulse on the ^{63}Cu channel to change the ^{63}Cu spin states adiabatically, which in turn depends on the nutation frequency ω_1. Using a dipolar evolution time of −0.94 ms ($14\tau_r$) and a recoupling pulse length of 33 μs ($\approx\tau_r/2$) at $\omega_1 = 83.3$ kHz signal losses of $16 \pm 1\%$ and $10 \pm 1\%$ were obtained for the resonances centered near −44 and 94 ppm, respectively, whereas they were found only near $3–4 \pm 1\%$ for the other signals. We thus conclude that the signals at −44 and 94 ppm correspond to the directly Cu-coordinated P1(P1′) and P2(P2′) sites. The difference between $10 \pm 1\%$ and $16 \pm 1\%$ probably reflects the fact that the large C_Q difference between the two Cu sites (≈30%) makes it impossible to adjust optimum REAPDOR conditions for both ^{31}P-^{63}Cu spin pairs simultaneously. A complementary approach to uncover the connectivities of the P_8Se_3 cage molecule is achieved employing the R-TOBSY sequence. In the case of $(CuI)_2P_8Se_3$, the optimum mixing time was adjusted to 2 ms according to a one-dimensional parameter optimization procedure. The resulting 2D-spectrum is presented in Fig. 9. Most significantly, the resonance centered at about $\delta = -44$ ppm clearly displays crosspeaks linking this resonance to all of the other NMR signals, suggesting ^1J spin–spin couplings and hence direct connectivity of the corresponding P atom to all of the other P sites. Therefore, we must assign this signal to the Cu-bonded P1(P1′) sites, whereas the resonance close to $\delta =$ 94 ppm belongs to the copper coordinated P2(P2′) sites, based on the REAPDOR result. The assignment of the remaining two resonances at 83.6 and 105.2 ppm to P3 or P4 remains ambiguous, because the complete interpretation of the crosspeak structure linking the three downfield resonances is impeded by the limited chemical shift resolution available. However, the assignment may be finalized in principle, if it were possible to reduce the peak overlap at significantly higher magnetic field strengths.

3. $(CuI)_3P_4Se_4$

The crystal structure of this compound is based on monomeric β-P_4Se_4 cages having C_s symmetry, which are embedded between columns of copper iodide. Three of the four phosphorus atoms are coordinated by copper, whereas selenium is exclusively bonded to phosphorus. In Fig. 10, a projection of the crystal structure is shown, illustrating the stacking of the β-P_4Se_4 cages along the *c*-axis. The coordination spheres for the copper atoms can be depicted as [$CuPI_3$]. Cu1 is centered within a distorted tetrahedron comprised of the phosphorus atom P1 and three iodine atoms. Cu2 and Cu3 are located within a tetrahedral environment of P4 and $3 \times$ I2 (Cu2), and P3 and $3 \times$ I3 (Cu3), respectively.

The ^{65}Cu MAS spectrum of $(CuI)_3P_4Se_4$ is shown in Fig. 11, including the fit to three distinct lineshape components reflecting the influence of second-order quadrupolar effects. The corresponding quadrupolar coupling constants extracted using the DMFIT program are summarized in Table 2. Based on the fact that the local environments for Cu2 and Cu3 are very similar, we attribute the broad resonance centered near 250

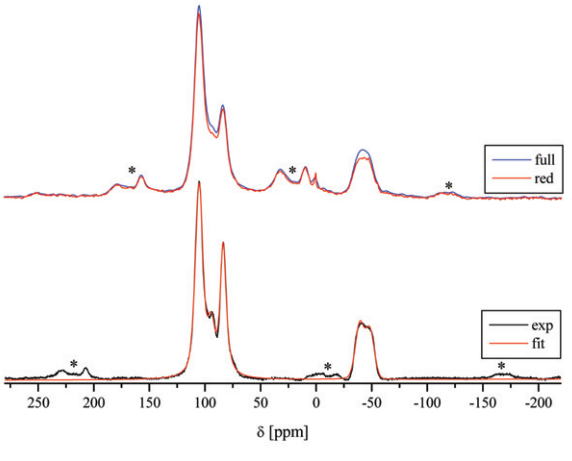

Fig. 8 ^{31}P-{^{63}Cu}-REAPDOR of $(CuI)_2P_8Se_3$ at 11.7 T (202.45 MHz) and a spinning frequency of 15 kHz with a recoupling pulse of 33 μs (≈half the rotor period) applied on the ^{63}Cu channel. The dipolar evolution time was set to 0.94 ms ($\approx 14\tau_r$) with $\omega_1(^{63}Cu) = 83.3$ kHz [blue: full spectrum without ^{63}Cu irradiation; red: reduced spectrum with ^{63}Cu irradiation.] The sharp peak next to 0 ppm indicates partial hydrolysis of the sample. At the bottom, the 25 kHz ^{31}P-MAS NMR spectrum at 11.7 T (202.45 MHz) is also shown. Spinning sidebands are marked with asterisks.

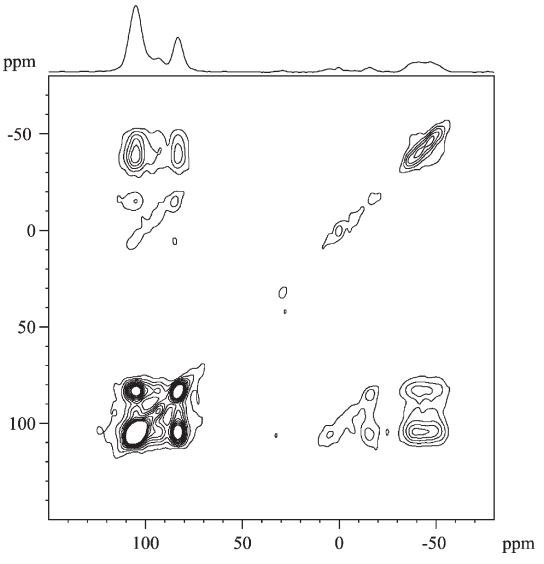

Fig. 9 ^{31}P-30 kHz MAS R-TOBSY spectrum of $(CuI)_2P_8Se_3$ at 11.7 T (202.49 MHz) under the following experimental conditions: $\tau_{mix} = 2.0$ ms, 102 t_1 increments at steps of 16.67 μs, relaxation delay 90 s. Ten positive contour levels between 2% and 30% of the maximum peak intensity were plotted. The F_2 projection is shown on the top.

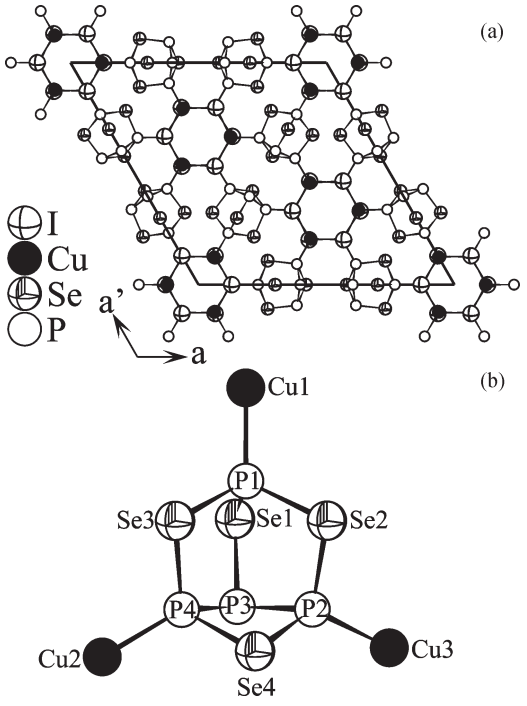

Fig. 10 (a) Projection of the crystal structure of $(CuI)_3P_4Se_4$ along [001]. The β-P_4Se_4 cages are stacked along the *c*-axis and surrounded by columns of CuI producing the motif of a hexagonal rod packing. (b) The labeling of the β-P_4Se_4 cage and its coordination to copper atoms.

ppm to these two Cu sites. This assignment is also consistent with the expectation that the least distorted site Cu1 gives rise to the NMR signal with the smallest quadrupolar coupling constant.

Fig. 12 shows the ^{31}P MAS-NMR spectrum, recorded at 303.59 MHz (17.6 T), demonstrating significantly enhanced resolution over the previously reported spectrum at 11.7 T.[13] At 17.6 T, the characteristic ^{31}P-$^{63,65}Cu$ scalar coupling multiplets associated with the Cu-bonded phosphorus atoms P1 and P2/P4 are adequately resolved whereas the resonances due to the chemically very similar P2 and P4 sites are strongly overlapping. Hence, taking into account the presence of both ^{63}Cu and ^{65}Cu isotopes, the full spectral deconvolution of the ^{31}P resonance multiplet structure requires six different multiplets. Table 2 summarizes the results obtained using the

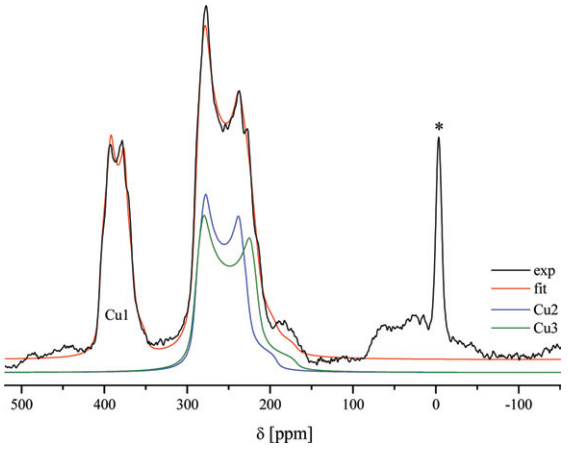

Fig. 11 ^{65}Cu MAS NMR spectrum of $(CuI)_3P_4Se_4$ at 11.7 T (142.00 MHz) and a spinning frequency of 30 kHz. The narrow peak marked with an asterisk indicates CuI impurity phase. The contributions of the two slightly distinct copper atoms Cu2 and Cu3 to the overall lineshape are also shown.

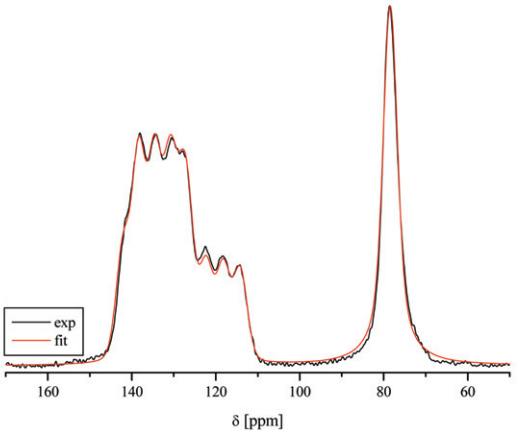

Fig. 12 ^{31}P MAS spectrum of $(CuI)_3P_4Se_4$ at 17.6 T (303.59 MHz) and a spinning frequency of 32.8 kHz. The spectrum was kindly provided by Prof. Eike Brunner (University of Regensburg).

WSOLIDS1 routine, which was applied in the same fashion as described above for $(CuI)P_4Se_4$, revealing excellent agreement with the experimental spectrum. Both the ^{31}P and the ^{65}Cu MAS-NMR spectra nicely confirm the proposed crystal structure especially emphasizing the presence of the novel molecular β-P_4Se_4 cages.

4. $(CuI)_3P_4S_4$

The structure of this material has similarities to the previously described selenium derivative and consists of monomeric β-P_4S_4 cage molecules that are separated by hexagonal columns of CuI. Two distinct fully occupied copper sites instead of three in the case of $(CuI)_3P_4Se_4$ were found. Again, three of the four phosphorus atoms are bonded to copper whereas no bonds between copper and sulfur are observed. The molecular structure of the β-P_4S_4 cage is found to be similar to those cages reported for the compound $[\beta\text{-}P_4S_4(NbCl_5)_2]$.[9] A projection of the crystal structure of $(CuI)_3P_4S_4$ along the *c*-axis as well as the labeling scheme for the β-P_4S_4 cage is presented in Fig. 13.[11]

Since the elements phosphorus and sulfur are hard to distinguish by X-ray diffraction methods due to their very similar scattering powers, comparison with structural results from complementary experimental techniques is desirable. The $^{63,65}Cu$ MAS spectra (*cf.* Fig. 14) show two well-resolved sites with an integrated area ratio of approximately 1:2, in agreement with the crystal structure. For both sites, the distortion from tetrahedral symmetry, as caused by Cu–P bonding, generates both a substantial downfield chemical shift relative to the chosen Cu-standard, solid CuI, and significant local electric field gradients at the copper sites.

The ^{31}P MAS-NMR spectrum of $(CuI)_3P_4S_4$, measured at 202.45 MHz is shown in Fig. 15. Based on the integrated area ratio of 1:2:1 as well as the peak multiplicity structure, an unambiguous peak assignment is possible attributing the narrow line at $\delta = 83.2$ ppm to the phosphorus site P3 while the copper-bonded sites P1 and P2 are identified due to their expected 1:2 area ratio. This assignment is confirmed further by a ^{31}P–$\{^{63}Cu\}$-REAPDOR experiment, which was conducted using a recoupling pulse length of 33 μs ($\approx\tau_r/2$) and a nutation frequency of $\omega_1 = 83.3$ kHz on the ^{63}Cu channel where the dipolar evolution time was set to ≈0.73 ms ($11\tau_r$). The resulting spectra (data not shown) reveal signal reductions of about $19 \pm 1\%$ (P1–Cu1) and $16 \pm 1\%$ (P2–Cu2), respectively. In contrast, the resonance associated with the phosphorus atom P3 nearly retains its original signal intensity ($\approx 2 \pm 1\%$ loss) in the REAPDOR experiments, because of its rather remote location from Cu atoms. A lineshape fit was

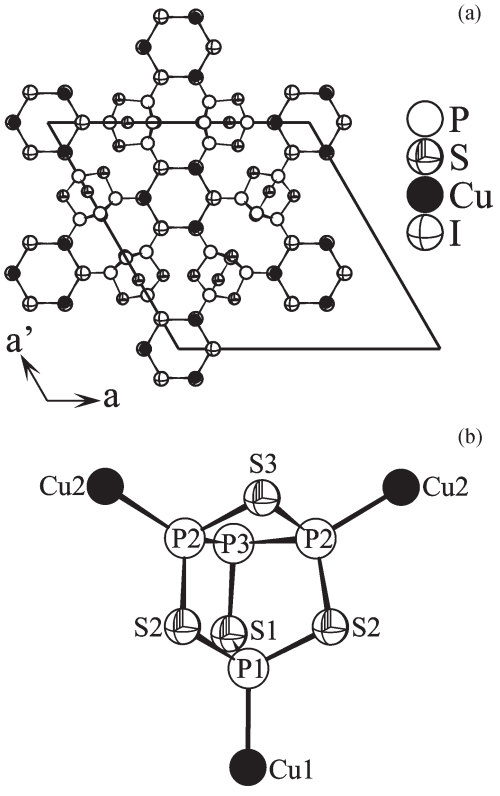

Fig. 13 (a) A projection of the crystal structure of $(CuI)_3P_4S_4$ along the *c*-axis illustrating the sixfold rotation axis parallel to *c*. The two distinct copper atoms are ordered and attached to the phosphorus atoms P1 and P2. (b) The labelling scheme of the β-P_4S_4 cage and its coordination to the copper atoms.

again obtained with the WSOLIDS1 routine, using the same procedure as described above for $(CuI)P_4Se_4$. All the simulation results are collected in Table 2.

According to the crystal structure, the presence of the copper(I) halide matrix does not affect the connectivity of the β-P_4S_4 cage itself. The latter can be studied in more detail using the R-TOBSY sequence. Figs. 16a and 16b show the 2D-correlation spectra recorded at two different mixing times. At short mixing times coherence transfer *via* ^1J coupling interactions is significantly emphasized, allowing the selective detection of the P2–P3 correlation based on direct bond connectivity. With an increased mixing time, the weaker scalar interactions (^2J)-P1–S1–P3 are also detected while the (^2J)-P2–S2–P1 crosspeaks have probably too small intensities because of the multiplet

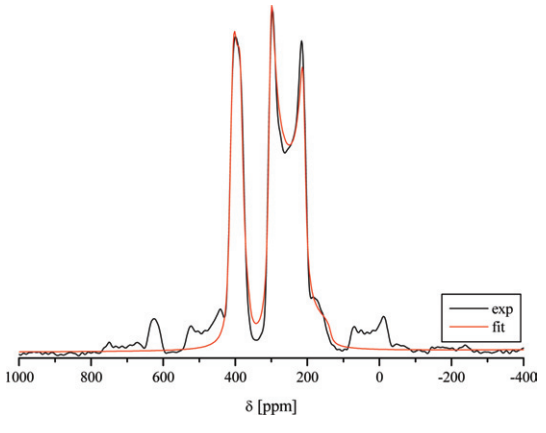

Fig. 14 ^{63}Cu MAS NMR spectrum of $(CuI)_3P_4S_4$ at 11.7 T (132.50 MHz) and a spinning frequency of 30 kHz. The minor peaks are spinning side bands.

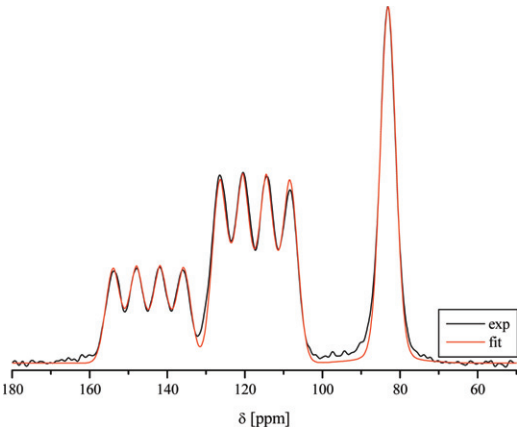

Fig. 15 ^{31}P MAS-NMR spectrum of $(CuI)_3P_4S_4$ at 11.7 T (202.45 MHz) and a spinning frequency of 30 kHz.

splittings involved. The square-shaped diagonal peaks associated with the copper-bonded P1 and P2 sites seem to suggest that 'autocorrelated' polarization transfer occurs. The nature of this process is indeed not too obvious. While for the site P2 a 'real' autocorrelation in the sense of scalar mediated polarization transfer would be possible (^2J-P2–S3–P2′), this is not feasible for the site P1. In the latter case the apparent 'autocorrelated' polarisation transfer is most likely an artifact caused by ^{63,65}Cu spin fluctuations due to spin-lattice interactions during the mixing time. As a result of such spin fluctuations, a fraction of those ^{31}P nuclei coupled to a given copper Zeeman state during the preparation period will be coupled to a different copper Zeeman state during the detection period, producing the apparent autocorrelation signal in the 2D-spectrum. Conceivably, this process also contributes to the square-shaped diagonal signal seen for the P2 site.

Discussion and Conclusions

While the above results have illustrated the inherent power of solid state NMR for the connectivity analysis of the phosphorus chalcogenide-copper iodide coordination compounds, this section focuses on the structural interpretation of the detailed ^{31}P and ^{63,65}Cu NMR Hamiltonian parameters, in relation to the interaction of the phosphorus chalcogenide molecules with the copper iodide matrix.

The *^{31}P chemical shifts* measured for the various phosphorus sites in the compounds studied here can be compared with published solution-state or solid-state NMR values obtained for the free cage molecules where possible. While β-P_4Se_4 and P_8Se_3 are hitherto unknown in the free, uncomplexed state, data are available for β-P_4S_4, ($\delta_{(P1)} = 174.7$ ppm, $\delta_{(P2)} = 207.5$ ppm and $\delta_{(P3)} = 85.7$ ppm[37]) and for α-P_4Se_4 ($\delta = 127$ ppm[38]). Inspection of Table 2 reveals that in each of these cases the coordination of a given P site with Cu(I) leads to pronounced upfield shift effects about 50 ppm in magnitude, whereas the chemical shifts of the non-Cu-bonded sites are barely affected. Given the fact that ^{31}P chemical shifts of phosphorus sulfide and selenide cages are otherwise extremely sensitive to small changes in the local phosphorus bonding geometry,[39] the results of the present study reveal that Cu^+ complexation causes electronic perturbations that are predominantly local and mostly confined to the directly-bonded P atoms. Thus, in agreement with the diffraction data, the NMR results indicate that the overall cage geometry in these inclusion compounds changes very little in relation to the free molecules.

The *isotropic ^{31}P-$^{63,65}Cu$ indirect spin–spin coupling constants* measured in this work can be compared to values previously obtained for the large family of copper(I)-triphenylphosphine

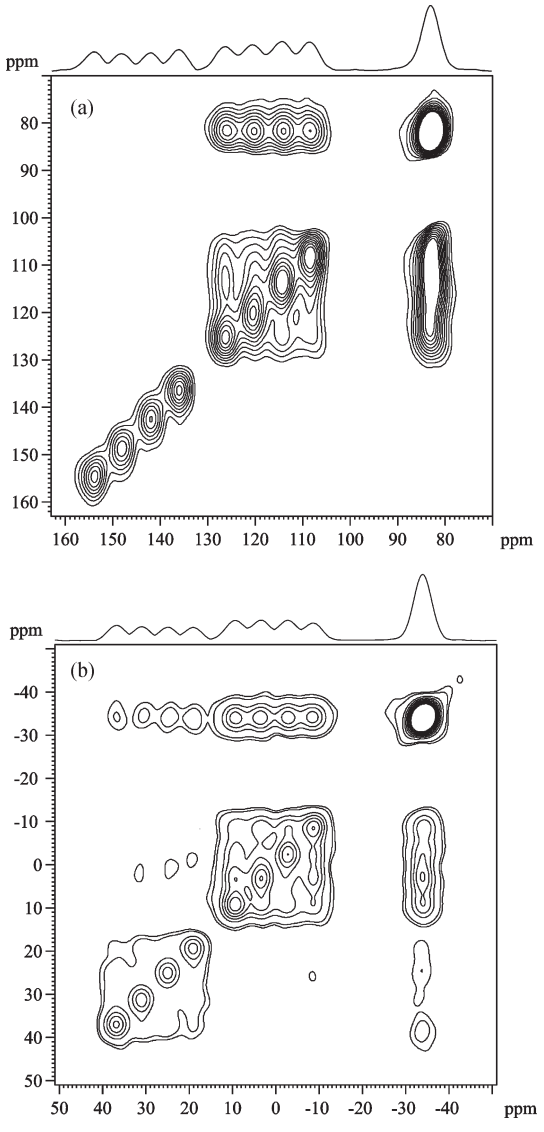

Fig. 16 (a) ^{31}P-25 kHz MAS R-TOBSY spectrum of $(CuI)_3P_4S_4$ at 11.7 T (202.47 MHz) under the following experimental conditions: $\tau_{mix} = 4.8$ ms, 62 t_1 increments at steps of 40 μs, relaxation delay 420 s. Quadrature detection in the F_1 dimension was achieved by the hypercomplex approach (STATES). Ten positive contour levels between 7% and 40% of the maximum peak intensity are plotted. The F_2 projection is shown on the top. (b) ^{31}P-30 kHz MAS R-TOBSY spectrum of $(CuI)_3P_4S_4$ at 11.7 T (202.47 MHz) under the following experimental conditions: $\tau_{mix} = 19.2$ ms, 70 t_1 increments at steps of 33.33 μs, relaxation delay 210 s. Quadrature detection in the F_1 dimension was achieved by the hypercomplex approach (STATES). Ten positive contour levels between 2% and 40% of the maximum peak intensity are plotted. The F_2 projection is shown on the top.

halide complexes representing the Cu local geometries $[CuP_{4-n}Hal_n]$, where $4 > n > 0$, and Hal = Cl,Br,I.[15,40–44] The coupling constants of these complexes are quite sensitive to the number n and the type of halide atoms attached to Cu, reflecting a good negative linear correlation ($R = 0.987$) between $^1J(^{31}P–^{63}Cu)$ and the copper–phosphorus distance $d_{(P–Cu)}$ (see Fig. 17). The copper halide adducts examined in the present work can be divided into two groups, namely those with $[CuPI_3]$ and those with $[CuP_2I_2]$ copper coordination spheres. While there still appears to be some correlation with $d_{(P–Cu)}$, the experimental data of $^1J(^{31}P–^{63,65}Cu)$ *vs.* $d_{(P–Cu)}$ fall significantly below the correlation line established for the triphenylphosphine halide complexes. For example, the $[CuPI_3]$-type compounds $(CuI)_3P_4S_4$ ($d_{(P–Cu)} = 222/224$ pm) and $(CuI)_3P_4Se_4$ ($d_{(P–Cu)} = 224$ to 227 pm) have coupling constants ranging from 1100 to 1210 Hz compared to values of

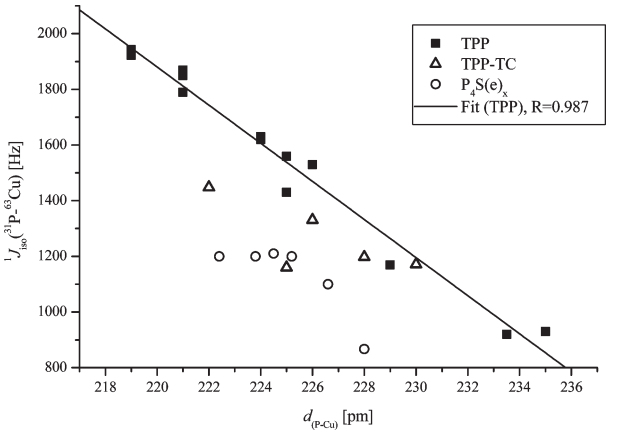

Fig. 17 Plot of $^1J_{iso}(^{31}P-^{63}Cu)$ *vs.* Cu-P distance $d_{P–Cu}$ for copper halide triphenylphosphine complexes, (TPP) for copper thiocarboxylate triphenylphosphine complexes, (TPP-TC) and for the compounds of the present study $(P_4S(e)_x)$.

1570–1700 Hz reported for the $[CuPI_3]$-type complex $[PPh_3CuI]_4$ (cube) ($d_{(P–Cu)} = 223$ pm) even though the internuclear distances are comparable. Similar ligand influences were previously observed for a series of Cu(I) triphenylphosphine thiocarboxylate complexes,[40] for which data have been included in Fig. 17 as well. Concerning the $[CuP_2I_2]$-type complex $(CuI)P_4Se_4$ ($d_{(P-Cu)} = 228$ pm) the coupling constant of 867 Hz also falls below the correlation line defined by the triphenylphosphine complexes. Additional J values (not included in Fig. 17) for the $[CuP_2Cl_2]$ coordination-type compound $[CuCl\{Cp^*Fe(\eta^5{:}\eta^1{:}\eta^1–P_5)\}]_\infty$ ($^1J(P–Cu) \approx 466 \pm 10$ Hz, $d_{(P–Cu)} = 227/229$ pm) and for $[CuBr\{Cp^*Fe(\eta^5{:}\eta^1{:}\eta^1{:}\eta^1–P_5)\}]_\infty$ ($^1J(P–Cu) \approx 560–780 \pm 10$ Hz, $d_{(P–Cu)} = 228/232$ pm) are even lower, reflecting the strong influence of the coordination ligand.[45]

A clear distinction of the various Cu coordination environments is given on the basis of the ^{63,65}*Cu isotropic chemical shifts*. Relative to the CuI standard (tetrahedral $[CuI_4]$ coordination), the $[CuPI_3]$ complexes resonate downfield near 300–400 ppm, while the $[CuP_2I_2]$ coordination environments are characterized by chemical shifts between 600 and 800 ppm downfield. For the five data points corresponding to the $[CuPI_3]$ environment, Fig. 18a suggests a correlation ($R = 0.98$) with the shear strain parameter

$$\chi = \sum_{i=1}^{6} \tan|\alpha_i - 109.48|$$

which can serve as a measure of distortion from the tetrahedral bonding geometry. In this expression the α_i are the six individual ligand–Cu–ligand angles, whose overall deviation from the ideal tetrahedral value is considered. Based on previous NMR studies of quadrupolar nuclei in distorted tetrahedral oxide geometries[46] it also appears reasonable to expect a correlation of the shear strain parameter with the ^{63,65}*Cu nuclear electric quadrupolar coupling constants*. While the electric field gradient vanishes for the regular tetrahedral sites in cubic CuI, the distortions produced by replacing one or two iodide ligands with P atoms result in C_Q-values ranging from 3 to 10 MHz in the present compounds. Within the range considered here, the C_Q-values appear to be weakly correlated with χ (with a correlation coefficient of 0.90) suggesting that the extension of this semi-empirical approach to the more covalent compounds of the present study is more limited. Still, it is worth noting that the linear least squares fit passes close to the theoretically expected data point $\{C_Q = 0, \chi = 0\}$, see Fig. 18b). The poor correlation between C_Q and χ is partly due to the fact that the length of the Cu–P bond, which is also expected to influence the electric field gradient at the copper

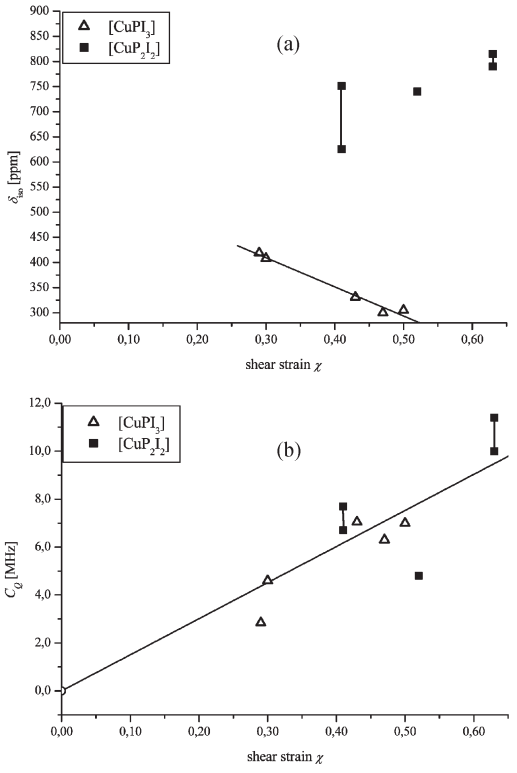

Fig. 18 (a) Plot of the experimental ^{63,65}Cu isotropic chemical shifts *versus* the empirical shear strain parameter χ. Vertical lines indicate the parameter uncertainty between the static and MAS-NMR fits to the ^{65}Cu spectra of $(CuI)_2P_8Se_3$. (b) Plot of the experimental ^{63}Cu quadrupolar coupling constants C_Q *versus* the empirical shear strain parameter χ. Vertical lines indicate the parameter uncertainty between the static and MAS-NMR fits to the ^{65}Cu spectra of $(CuI)_2P_8Se_3$.

sites, shows considerable variations (222 to 228 pm) for the Cu sites within the series of compounds examined here. Considering the fact that the copper-iodine atomic distances lie between 255 and 265 pm, a lengthening of the P–Cu bonds is expected to produce a more symmetrical electron distribution around copper and hence reduce the C_Q-values. In spite of the more complicated situation weakening the C_Q *vs.* χ correlation here, our results suggest that it can still serve as a guide for ^{63}Cu signal assignments in each given compound when multiple Cu sites are present. Further quantitative insights should be sought not from semi-empirical considerations but rather from quantum-chemical field gradient calculations.

Acknowledgements

Generous funding of this work by the DFG and the Wissenschaftsministerium NRW is most gratefully acknowledged. G. B. thanks the Fonds der Chemischen Industrie for a doctoral stipend. We thank Professor Eike Brunner (University of Regensburg) for providing the ^{31}P MAS-NMR spectrum of $(CuI)_3P_4Se_4$, which was recorded at the 17.6 T spectrometer available at the University of Leipzig.

References

1 A. Pfitzner, *Chem. Eur. J.*, 2000, **6**, 1891.
2 A. Freudenthaler and A. Pfitzner, *Solid State Ionics*, 1997, **101–103**, 1053.
3 A. W. Cordes, R. D. Joyner, R. D. Shores and E. D. Dill, *Inorg. Chem.*, 1974, **13**, 132.
4 M. Di Vaira, M. Peruzzini and P. Stoppioni, *J. Chem. Soc., Dalton Trans.*, **1985**, 291.
5 M. Di Vaira, M. Peruzzini and P. Stoppioni, *J. Chem. Soc., Chem. Commun.*, **1983**, 903.
6 M. Di Vaira, M. Peruzzini and P. Stoppioni, *J. Organomet. Chem.*, 1983, **258**, 373.
7 M. Di Vaira, M. Peruzzini and P. Stoppioni, *Inorg. Chem.*, 1983, **22**, 2196.
8 A. Adolf, M. Gonsior and I. Krossing, *J. Am. Chem. Soc.*, 2002, **124**, 7111.
9 H. Nowottnick, K. Stumpf, R. Blachnik and H. Reuter, *Z. Anorg. Allg. Chem.*, 1999, **625**, 693.
10 A. Pfitzner, S. Reiser and H. J. Deiseroth, *Z. Anorg. Allg. Chem.*, 1999, **625**, 2196.
11 S. Reiser, G. Brunklaus, J. H. Hong, J. C. C. Chan, H. Eckert and A. Pfitzner, *Chem. Eur. J.*, 2002, **8**, 4228.
12 A. Pfitzner, S. Reiser and T. Nilges, *Angew. Chem. Int. Ed. Engl.*, 2000, **39**, 4160.
13 A. Pfitzner and S. Reiser, *Inorg. Chem.*, 1999, **38**, 2451.
14 E. M. Menger and W. S. Veeman, *J. Magn. Reson.*, 1982, **46**, 257.
15 A. C. Olivieri, *J. Am. Chem. Soc.*, 1992, **114**, 5758.
16 T. Gullion, *J. Magn. Reson.*, 1995, **A 117**, 326.
17 A. E. Bennett, R. G. Griffin and S. Vega, *NMR Basic Principles and Progress*, 1994, **33**, 1.
18 S. Dusold and A. Sebald, *Annu. Rep. NMR Spectroscop.*, 2000, **41**, 185.
19 M. Baldus and B. H. Meier, *J. Magn. Reson. A*, 1996, **121**, 65.
20 M. Baldus, R. J. Iuliucci and B. H. Meier, *J. Am. Chem. Soc.*, 1997, **119**, 1121.
21 S. Dusold, J. Kümmerlen and A. Sebald, *J. Chem. Phys. A*, 1997, **101**, 5895.
22 A. Lesage, C. Auger, S. Caldarelli and L. Emsley, *J. Am. Chem. Soc.*, 1997, **119**, 7867.
23 R. Verel, J. D. van Beek and B. H. Meier, *J. Magn. Reson.*, 1999, **140**, 300.
24 A. Lesage, M. Bardet and L. Emsley, *J. Am. Chem. Soc.*, 1999, **121**, 10 987.
25 X. Helluy, C. Marichal and A. Sebald, *J. Phys. Chem. B*, 2000, **104**, 2836.
26 E. H. Hardy, R. Verel and B. H. Meier, *J. Magn. Reson.*, 2001, **148**, 459.
27 A. S. D. Heindrichs, H. Geen, C. Giordani and J. J. Titman, *Chem. Phys. Lett.*, 2001, **335**, 89.
28 M. Carravetta, M. Edén, X. Zhao, A. Brinkmann and M. H. Levitt, *Chem. Phys. Lett.*, 2000, **321**, 205.
29 A. Brinkmann and M. H. Levitt, *J. Chem. Phys.*, 2001, **115**, 357.
30 J. C. C. Chan and G. Brunklaus, *Chem. Phys. Lett.*, 2001, **349**, 104.
31 M. Bak, J. T. Rasmussen and N. C. Nielsen, *J. Magn. Reson.*, 2000, **147**, 296.
32 G. Brunklaus, PhD Dissertation, Münster, 2003.
33 D. Massiot, F. Fayon, M. Capron, I. King, S. Le Calvé, B. Alonso, J.-O. Durand, B. Bujoli, Z. Gan and G. Hoatson, *Magn. Reson. Chem.*, 2002, **40**, 70.
34 K. Eichele, R. Wasylishen, WSOLIDS1 V. 1. 17.34, Dalhousie University, 2001; K. Eichele, R. Wasylishen, *Inorg. Chem.*, 1994, **33**, 2766.
35 M. H. Levitt, in *Supplement to the Encyclopedia of Nuclear Magnetic Resonance*, eds., D. M. Grant and R. K. Harris, Wiley, 1996, in press.
36 D. J. States, R. A. Haberkorn and D. J. Ruben, *J. Magn. Reson.*, 1982, **48**, 286.
37 A. M. Griffin, P. C. Minshall and G. M. Sheldrick, *J. Chem. Soc., Chem. Commun.*, 1976, 809.
38 D. Lathrop and H. Eckert, *J. Phys. Chem.*, 1989, **93**, 7895.
39 H. Eckert, C. S. Liang and G. D. Stucky, *J. Phys. Chem.*, 1989, **83**, 452.
40 F. Asaro, A. Camus, R. Gobetto, A. C. Olivieri and G. Pellizer, *Solid State Nucl. Magn. Reson.*, 1997, **8**, 81.
41 P. C. Healy, A. K. Whittaker, J. D. Kildea, B. W. Skelton and A. H. White, *Austr. J. Chem.*, 1991, **44**, 729.
42 G. A. Bowmaker, A. Camus, P. C. Healy, B. W. Skelton and A. H. White, *Inorg. Chem.*, 1989, **28**, 3883.
43 G. A. Bowmaker, B. W. Skelton, A. H. White and P. C. Healy, *J. Chem. Soc. Dalton Trans.*, 1988, 2825.
44 S. Kroeker, J. V. Hanna, R. E. Wasylishen, E. W. Ainscough and A. M. Brodie, *J. Magn. Reson.*, 1998, **135**, 208.
45 G. Brunklaus, H. Eckert and M. Scheer, to be published.
46 M. T. Weller, M. E. Brenchley, D. C. Apperley and N. A. Davies, *Solid State Nucl. Magn. Reson.*, 1994, **3**, 103.